ILT for Double Exposure Lithography with Conventional and Novel Materials

Amyn Poonawala[a] and Yan Borodovsky[b] and Peyman Milanfar[c]

[a]Department of Computer Engineering, University of California, Santa Cruz, USA
[b]Portland Technology Development, Intel Corporation, Hillsboro, USA
[c]Department of Electrical Engineering, University of California, Santa Cruz, USA

ABSTRACT

Multiple paths exists to provide lithography solutions pursuant to Moore's Law for next 3-5 generations of technology, yet each of those paths inevitably leads to solutions eventually requiring patterning at $k_1 < 0.30$ and below. In this article, we explore double exposure single development lithography for $k_1 \geq 0.25$ (using conventional resist) and $k_1 < 0.25$ (using new out-of-sight out-of-mind materials). For the case of $k_1 \geq 0.25$, we propose a novel double exposure inverse lithography technique (ILT) to split the pattern. Our algorithm is based on our earlier proposed single exposure ILT framework, and works by decomposing the aerial image (instead of the target pattern) into two parts. It also resolves the phase conflicts automatically as part of the decomposition, and the combined aerial image obtained using the estimated masks has a superior contrast.

For the case of $k_1 < 0.25$, we focus on analyzing the use of various dual patterning techniques enabled by the use of hypothetic materials with properties that allow for the violation of the linear superposition of intensities from the two exposures. We investigate the possible use of two materials: contrast enhancement layer (CEL) and two-photon absorption resists. We propose a mathematical model for CEL, define its characteristic properties, and derive fundamental bounds on the improvement in image log-slope. Simulation results demonstrate that double exposure single development lithography using CEL enables printing 80nm gratings using dry lithography. We also combine ILT, CEL, and DEL to synthesize 2-D patterns with $k_1 = 0.185$. Finally, we discuss the viability of two-photon absorption resists for double exposure lithography.

Keywords: Double exposure lithography, inverse lithography, CEL, two-photon absorption resist, ILS.

1. INTRODUCTION AND BACKGROUND

Double exposure lithography is considered an important road-map enabler for 32nm and smaller nodes. Double exposure can be broadly classified into two categories depending on the number of times the resist is developed. In the single development case, two (same or different) masks and two (same or different) illumination settings are used in order to print the desired circuit pattern. If a conventional resist is used, the final aerial image is the linear super-position of the two individual exposures. Hence, the minimum resolvable pitch is the same as single-exposure, i.e., minimum $k_{pitch} = 0.5$ and

$$\text{Min Pitch} = 0.5\frac{\lambda}{NA}. \tag{1}$$

The above technique is known to give superior contrast for low k_1 values and finds applications such as trim mask with alternating phase shift masks (PSM),[5] double dipole lithography, IDEAL (Innovative Double Exposure by Advanced Lithography),[7] etc.

The double development case (also referred to as dual patterning) requires an additional resist development, etching, and coating steps in between the two exposures.[4,8] The concept behind multiple exposure/develop

[a] E-mail: amyn@ce.ucsc.edu
[b] E-mail: yan.borodovsky@intel.com
[c] E-mail: milanfar@ee.ucsc.edu

techniques is that the fundamental single-exposure limit given in (1) is not on the individual feature size (CD), but on the pattern pitch.[1] Using non-linearities in the pattern transfer process, CDs can be much smaller than the half of the smallest allowed pitch. Dual patterning uses the above concept by patterning features at dimensions close to 1/4 of the minimal pitch allowed by constrains of imaging system, and stores the information from the first exposure in a hard mask (or other sacrificial layer). The second exposure is then carried out with similar feature size target and appropriate shift and again preserved in sacrificial layer, thereby doubling the frequency of each exposed features present on each of the masks. The minimum pitch resolution for dual patterning is $0.25\frac{\lambda}{NA}$. It was demonstrated that dual patterning allows one to reach patterning with effective k_1 as low as 0.16.[12]

However, additional processing steps related to preserving image of the first exposure in sacrificial layer (such as need to load and unload wafer twice from the exposure tool), carry additional overlay and dimensional control (CD) penalty. Furthermore, the extra processing steps such as second develop, hard-mask deposition, and etch steps might result in additional yield liability as well as increased wafer cost. There is strong incentive to identify techniques capable to support patterning with two masks containing split design information, yet capable of producing combined final latent image in resist without unloading the wafer off the exposure tool chunk. We thus need only one single exposure to produce image ready for *pitch doubling*, thereby avoiding the need for sacrificial layer, the follow-up processing steps, and their corresponding yield liabilities.

In this article, we exclusively focus on double exposure single development lithography (hence referred to as DEL). The paper considers two cases of DEL. The first case employs DEL to pattern with high contrast logic pattern at low k1 values between 0.25 and 0.35 with conventional type resist. DEL involves decomposing the pattern into two parts. Such decompositions are typically carried out using rule-based techniques or using H and V decomposition. In the latter case, the horizontal features of the pattern are printed during the first exposure using a Y-dipole illumination. The above illumination suppresses the features along the vertical direction. The second exposure uses a X-dipole illumination and accounts for the vertical features. The above decomposition needs to be performed along with model-based OPC to guarantee that the corners and junctions are accurately reproduced.[2] In this paper, we propose a novel inverse lithography (ILT) based approach for (input) mask design. The key feature of DEL-ILT is that it acts by decomposing the (gray level) aerial image and not the (binary) target pattern into two parts. The final aerial image has high contrast and uniform intensity in all the regions. We present discussion on chromeless phase-shift (CPL) mask design for coherent imaging systems. However, the framework can be extended to OPC, EPSM, and AltPSM, as well as to partially coherent imaging systems, without significant negative impact on computational efficiency or loss of framework generality.

The second case is an ambitious paradigm of DEL for $k_1 < 0.25$. Considering the single development scenario, the only way this is possible is by using new out-of-sight out-of-mind (OSOM) materials with properties that allow non-linear combination of the two aerial images obtained from the individual exposures. We have identified two potential candidates with regard to above which are discussed in this article. The first one is called CEL (contrast enhancement layer) which was originally proposed in 1980s in an effort to improve the resist profiles for single exposure lithography.[10,11] We propose a mathematical model for CEL and suggest key properties and parameters which will make such material conducive to DEL use below $k_1 < 0.25$. We also compare the performance of the proposed phenomenological model for CEL DEL material with characteristics of novel bleachable material kindly provided by Pixelligent Inc. We then explain the working of CEL for 80nm grating using dry lithography with $k_{pitch} = 0.34$, and the trade-offs involved for achieving high image-log-slope of the transmitted dose. Finally, we extend the ILT framework in order to synthesize 2D patterns with $k_1 < 0.25$ using CEL for DEL. The second OSOM material is two-photon absorption resist which responds to the square of the intensity of the aerial image. We discuss its suitability for DEL (1D case) and the major shortcoming which makes it practically infeasible.

In Section 2 we introduce a novel DEL ILT algorithm for $k_1 \geq 0.25$. The proposed CEL model and its usage for the 1-D case are presented in Section 3. In Section 4 we present three potential ways to improve the ILS using CEL. DEL, CEL, and ILT are combined together to enable 2-D patterning for $k_1 < 0.25$ in Section 5, and the two-photon absorption resist is discussed in Section 6. Finally, we provide conclusive remarks in Section 7.

2. DOUBLE EXPOSURE INVERSE LITHOGRAPHY FOR $K_1 \geq 0.25$

In this section we use DEL with conventional photo-resist, and discuss the ILT framework for automatic pattern decomposition and mask design.

2.1. Inverse Lithography Technology

Our DEL-ILT algorithm is built on the previously proposed single exposure ILT framework. In what follows, we provide a brief overview of inverse lithography technology.

Inverse lithography attempts to synthesize the mask (input) which leads to the desired wafer pattern (output) by inverting the forward model from mask to wafer.[21,22] The mask ($\underline{\mathbf{m}}$) synthesis problem is defined as an optimization problem where the cost function is defined as the L_2 norm of the distance between the target pattern ($\underline{\mathbf{z}}^*$) and the output ($\underline{\mathbf{z}}$). The latter can be modeled as the aerial image, the resist contour, or the etched contour depending on the correction goal. Authors have already established an ILT framework that maximizes aerial image contrast and/or reduces deviation of modeled resist contours from target locations.[19,20] Our technique is based on continuous function formulation and employs first-order gradient based optimization routines to estimate the mask. The gradient information enables systematic exploration of the solution space instead of the previously employed discrete domain,[9,23] random perturbation,[13] and evolutionary algorithm[3] based techniques. We also make use of the regularization framework to control the tone and complexity of the estimated masks [*]. The computational complexity of our algorithm is $O(MN\log(MN))$ for an $M \times N$ sampled pattern.

2.2. DEL-ILT

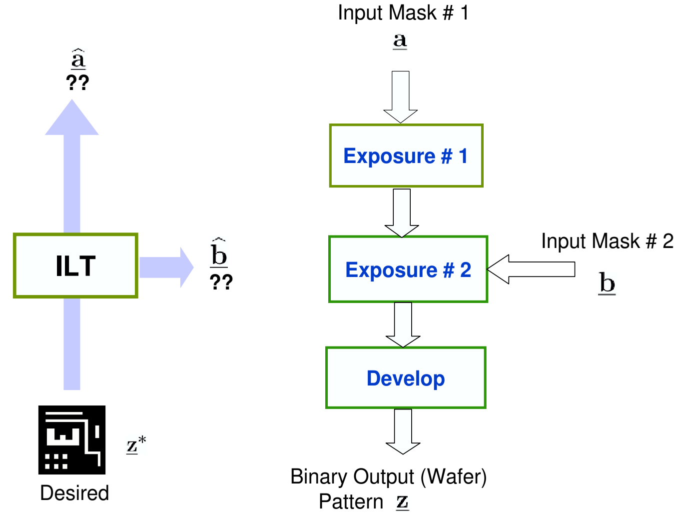

Figure 1. Forward Model and ILT for Double Exposure Lithography Systems

Fig. 1 illustrates the forward model as well as the inverse mask design problem for DEL. The input masks $\underline{\mathbf{a}}$ and $\underline{\mathbf{b}}$ are exposed using same or different imaging settings. The exposure energies are added in the resist which is finally developed to obtain the contours. The ILT routine starts with the target pattern $\underline{\mathbf{z}}^*$ and aims to estimate both the input masks $\hat{\underline{\mathbf{a}}}$ and $\hat{\underline{\mathbf{b}}}$. To keep things simple, we are currently restricting ourselves to estimating resist contours through simple aerial image thresholding, thus implying resist with very high contrast and neglecting other resist effects. Furthermore, we assume that both exposures employ the same imaging conditions (fully coherent with $\sigma = 0$). Under the above assumptions, the forward model can be defined as,

$$\underline{\mathbf{z}} = |\mathbf{H}\underline{\mathbf{a}}|^2 + |\mathbf{H}\underline{\mathbf{b}}|^2, \tag{2}$$

[*] For a detailed explanation on the need and procedure of the regularization framework for ILT, please refer to the literature[18–20]

where $\mathbf{H}$ represents a *jinc* function with cutoff frequency NA/λ. The mask synthesis problem can be formulated as minimizing the L_2 norm of the difference between the desired pattern $\underline{\mathbf{z}}^*$ and the aerial image $\underline{\mathbf{z}}$ defined in (2),

$$[\widehat{\underline{\mathbf{a}}}, \widehat{\underline{\mathbf{b}}}] = \arg\min_{\underline{\mathbf{a}},\underline{\mathbf{b}}} F(\underline{\mathbf{a}}, \underline{\mathbf{b}}) = \arg\min_{\underline{\mathbf{a}},\underline{\mathbf{b}}} ||\underline{\mathbf{z}}^* - |\mathbf{H}\underline{\mathbf{a}}|^2 - |\mathbf{H}\underline{\mathbf{b}}|^2||_2^2. \tag{3}$$

In order to allow for solutions permitting use of phase shifting masks, the above optimization problem is subject to bound constraints

$$-1 \le a_j \le 1 \;\text{ and }\; -1 \le b_j \le 1 \text{ for } j = 1, \ldots, MN\ . \tag{4}$$

Furthermore, the tone of the estimated masks can be controlled by employing the regularization framework and using a quadratic penalty term. A detailed discussion on double exposure ILT can be found in the literature.[17] We calculate the gradient of (3) with respect to $\underline{\mathbf{a}}$ and $\underline{\mathbf{b}}$ and update the masks in a cyclic coordinate fashion as follows:

$$\underline{\mathbf{a}}^{k+1} = \underline{\mathbf{a}}^k - s_1 \nabla_{\underline{\mathbf{a}}} F_1(\underline{\mathbf{a}}^k, \underline{\mathbf{b}}^k) \tag{5}$$

$$\underline{\mathbf{b}}^{k+1} = \underline{\mathbf{b}}^k - s_2 \nabla_{\underline{\mathbf{b}}} F_1(\underline{\mathbf{a}}^{k+1}, \underline{\mathbf{b}}^k) \tag{6}$$

2.3. Results

We now discuss some simulation results obtained using the proposed DEL-ILT algorithm.

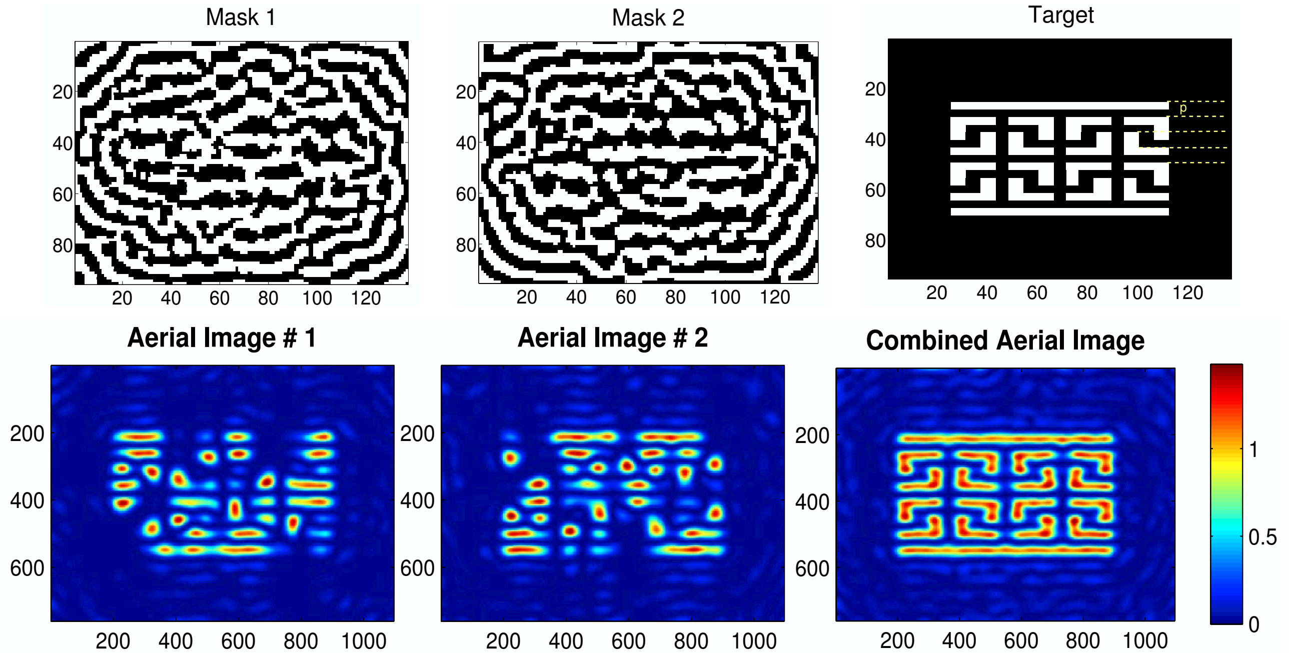

Figure 2. Top row illustrates the estimated CPL masks (black=-1 and white=+1) and the (binary) target pattern consisting of 60nm features. The pitch p=120nm is indicated by dotted lines in the figure. Bottom row indicates the aerial images for the individual exposures and the combined aerial image. Here $NA = 0.93$ and $k_1 = 0.289$.

Our first experiment is to print the complex pattern consisting of 60nm features (as indicated in Fig. 2) using 193/0.93NA dry lithography. The mask pixel size is 20nm in wafer dimensions (actual size 80nm for a 4X reduction system). The estimated CPL masks were obtained by optimizing (3) using the steepest-descent algorithm discussed in Section 2.2. The aerial images calculated using the estimated masks are illustrated in the bottom row in Fig. 2, and indicate very interesting pattern decomposition. The DEL-ILT algorithm splits the aerial image into two (overlapping) parts, each suitable for printing by the individual exposure. In the process

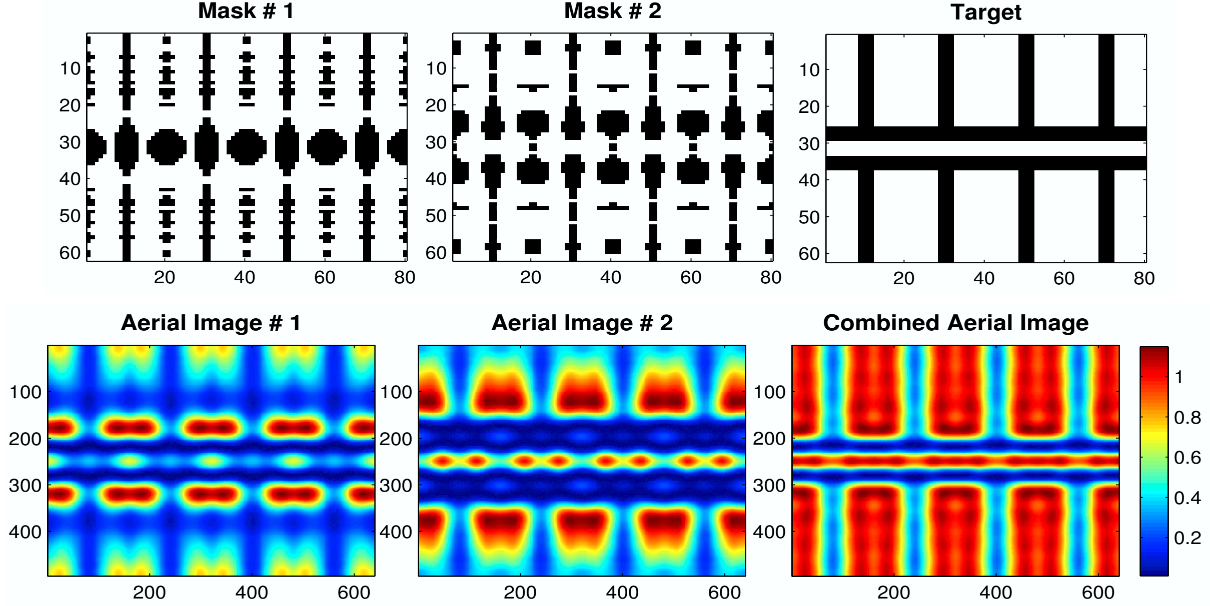

Figure 3. Top row illustrates the estimated CPL masks and the target pattern consisting of 80:320 vertical grating interlaced with 80nm wide horizontal features. Bottom row indicates the aerial images for the individual exposures and the combined aerial image. Here $NA = 0.85$ and $k_1 = 0.35$.

it automatically resolves all the possible phase-conflicts. The combined aerial image has very good quality and closely resembles the target pattern.

In the next experiment, our goal is to print the target illustrated in Fig. 3 consisting of 80:320 vertical gratings (thin lines in between large spaces). Here the pixel-size is 20nm, $NA = 0.85$, radiation wavelength = 193nm with corresponding $k_1 = 0.35$ for smallest pattern pitch. The target also consists of a 80nm horizontally sandwiched space thereby making whole layout a challenging patterning problem. The estimated CPL masks obtained using DEL-ILT along with their corresponding aerial images are illustrated in Fig. 3. We again observe an unconventional pattern decomposition, but the combined aerial image has very good contrast. In particular, note that there is a very well-defined separation (dark-area) between the horizontal space and grating line-ends; something very challenging to obtain using conventional H-V decomposition.

In conclusion, the DEL-ILT framework leads to un-intuitive but highly effective pattern decompositions. Unlike the commonly employed paradigm of splitting the (binary) target pattern, DEL-ILT aims to decompose the (gray-level) aerial image. We also note that mask design for DEL is an ill-posed problem. Therefore, the pattern decompositions illustrated in Fig. 2 and Fig. 3 are not necessarily unique. In general there may be multiple ways of splitting the patterns for double exposure. The *preferred decomposition* can be arrived at using the regularization framework. For example, a critical requirement for DEL is the robustness to mask-alignment errors. The above can be incorporated as a regularization function in order to obtain DEL masks which are also tolerant to misalignment. This forms an important direction of future research.

3. DEL USING CONTRAST ENHANCEMENT LAYER (CEL) FOR $K_1 < 0.25$

We now move on to the case of $k_1 < 0.25$ and discuss CEL as a potential technology enabler for the above case. Contrast enhancement layer (CEL) is a photo-bleachable film which is coated on top of the conventional photo-resist. It was studied in the 1980s in order to improve the sidewall angle of single exposure lithography process.[6, 10, 11, 15] The CEL film is initially unbleached with (ideally) zero or very low transmittance for small dose values. As the incident dose increases, the film starts undergoing bleaching action and the transmittance increases. The bleaching rate is related to the incident energy. The transmittance of an ideal fully bleached CEL

film is equal to one. Thus, the film which was initially opaque to the exposure wavelength, becomes transparent upon exposure. When the aerial image is incident on the CEL, higher intensity regions bleach faster compared to lower intensity ones. This non-linear transformation of the incident aerial image leads to a higher contrast of the dose received by the resist. During the exposure, the unbleached portion of the CEL will act as a portable conformable mask. Finally, we want to point out that our current model takes a simplified view and ignores the reflections from the substrate.

3.1. Modeling

The (non-ideal) bleaching behavior of the CEL is similar to a soft-threshold operation. Therefore, the CEL film transmittance $T(D_i)$ can be modeled as a sigmoid function as follows,

$$T(D_i) = \text{sig}(D_i, a, t_c, c) = \frac{1}{1 + e^{-acD_i + at_c}}, \tag{7}$$

where D_i is the incident dose, parameter c is inversely related to the thickness, a is related to the slope of the transition region, and t_c is the threshold dose parameter of the sigmoid. Fig. 4 indicates the behavior of a typical sigmoid function with $a = 60$, $t_c = 0.15$, and varying values of c. As discussed earlier, the transmittance is low for small values of incident dose. As the input dose builds up, the film starts bleaching and its transmittance increases ($T(D_i) = 0.5$ for $D_i = t_c/c$). Fig. 4 also indicates the effect of the film thickness c on the film transmittance. A thin CEL film bleaches quickly compared to a thicker one, and hence has a steeper transition region. Furthermore, a thick CEL film also requires higher dose values to become fully transmissive.

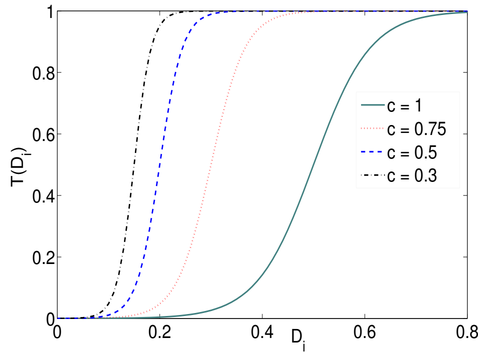

Figure 4. CEL film transmittance for different film thickness.

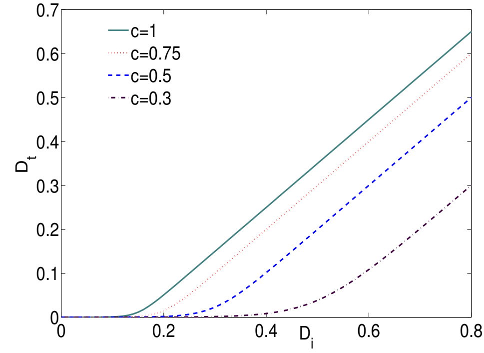

Figure 5. Transmitted dose (D_t) versus input dose D_i for different film thickness.

The final transmitted dose $D_t\{D_i\}$ (henceforth referred to as simply D_t), is obtained by integrating the transmittance as the incident dose builds up from 0 to D_i.

$$D_t = \int_0^{D_i} T(D_i) dD_i = \int_0^{D_i} \frac{1}{1 + e^{-acD_i + at_c}} dD_i$$

Therefore,

$$D_t = D_i - \frac{t_c}{c} + \frac{1}{ac} \log \left[1 + e^{(-acD_i + at_c)}\right] \tag{8}$$

Fig. 5 indicates that the graph of transmitted dose versus incident dose consists of three regions. For low doses (unbleached film), the incident dose is absorbed by the CEL film and D_t is very low. When D_i increases, the film starts bleaching and there is a non-linear increase in the transmitted energy. Finally, the CEL film gets fully bleached after which the transmitted dose increases linearly. As one would expect, the above regions also depend on the thickness of the CEL film. Thinner CEL films enter the linear region earlier compared to the thicker ones.

3.2. Working of CEL

We now discuss the working of CEL for the simple example of 1-D gratings. The target consists of 80nm (1:1) grating which needs to be printed using 193/0.85NA ($k_{pitch} = 0.35$). The first step is to divide the target into two 160nm pitch gratings which can be printed using single exposure CPL masks (with pitch = 320nm). Note that the second exposure consists of simply shifting the mask by 80nm. The leftmost plot in Fig. 6 indicates the aerial image and the transmitted CEL image (calculated using (8)), both for the first exposure. The CEL transmitted dose is absorbed by the photoresist and stored in the form of PAC (photo-active compound) concentration. The center plot indicates the aerial image and the CEL dose for the second exposure. It is very important to highlight here that in order to support DEL, the CEL considered should have *reversible bleaching* property. In other words after the first exposure is completed, the entire CEL film returns back to its original (opaque) state. If the CEL were not reversible, the regions previously exposed would remain bleached and as such have different transmittance values than those indicated in Fig. 4. Development of the above material is central to the use of CEL for double exposure. Such materials are not just hypothetical as is evidenced by class of reversible CEL (Arsel $^{\mathrm{TM}}$) under development by Pixelligent Inc.

The total dose absorbed by the resist is a superposition of the two CEL transmitted doses. The rightmost graph in Fig. 6 indicates that the combined transmitted CEL dose (assuming the reversibility property) shows good modulation. An intuitive explanation is that the CEL suppresses the aerial image energy in the unwanted regions owing to the soft-thresholding action. This has the effect of truncating the tail of the optical PSF (making it narrower), and resulting in less energy being deposited in the areas targeted by the second exposure. Fig. 6 also indicates the aerial image in the absence of CEL layer (just for demonstration purpose). Since $k_{pitch} < 0.5$, no useful modulation is observed.

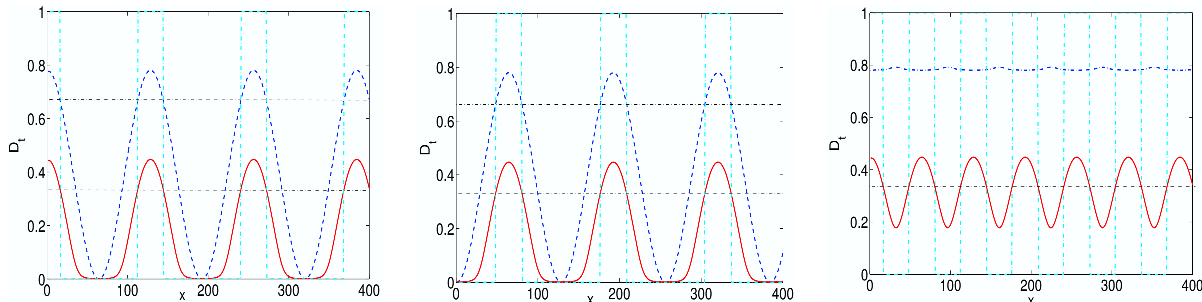

Figure 6. The left and center figures indicate the aerial images and the CEL images for the two individual exposures. The figure on the right indicates the combined aerial image (showing no modulation) and the combined CEL image (showing good modulation). In this case $a = 30$, $t_c = 0.15$, and $c = 0.45$.

The image log-slope (ILS) calculated at the desired edge location (CD = 40nm) for the incoming aerial image (D_i) and the CEL image (D_t) are 0.016 and 0.032 respectively. Thus the CEL also improves the aerial image contrast which was indeed one of the earliest applications of CEL.[14] Finally, we also observe that the transmitted CEL doses have lower magnitude compared to the incoming (aerial image) dose. We discuss this in more detail in the next section.

4. IMPROVING ILS OF THE CEL IMAGE

Our goal now is to improve the robustness of the double exposure CEL-based lithography system. This will also enable us to understand the fundamental trade-offs involved in designing a CEL-DEL system. We have identified three potential ways to improve the operating ILS at the desired edge location which are discussed below. The experimental setup employed here is the same as in Section 3.

4.1. CEL Film Thickness

The effect of the CEL film thickness parameter c on the film transmittance and the transmitted dose were illustrated earlier in Fig. 4 and Fig. 5 respectively. Fig. 7 illustrates the effect of c on the transmitted dose modulation assuming a fixed value of the incoming (aerial image) dose modulation D_i. The remaining simulation parameters are fixed ($a = 30$, $t_c = 0.15$), and c was varied from 0.8 to 0.2. We observe that as the CEL film becomes thicker, the magnitude of the transmitted dose modulation decreases. Therefore, in order to obtain 40nm CD, the photo-resist threshold t_r should be equal to 0.48, 0.36, and 0.076 for $c = 0.8, 0.5$, and 0.2 respectively. The ILS value for the corresponding t_r values is 0.022, 0.03, and 0.054. To summarize, the ILS can be improved by using a thicker CEL film. However, patterning the above image also requires very sensitive (high-acid generating) resists, having very low t_r value.

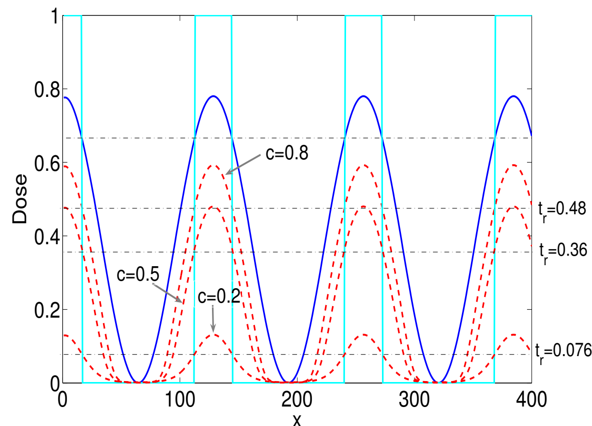

Figure 7. Effect of CEL film thickness assuming fixed D_i.

4.2. Incoming Dose Magnification

The second mode of operation is to use the same photoresist (fixed value of t_r), and magnify the incoming dose by a factor p. The CEL film thickness c also needs to be adjusted in order to match D_t with the target CD at the chosen threshold value t_r. Fig. 8 illustrates the original aerial image (D_i) and the transmitted CEL doses for four different values of p assuming a resist with operating threshold $t_r = 0.33$. The corresponding CEL thickness parameters are also indicated in the legend. We observe that as the dose magnification increases, the transmitted CEL image quality improves. The ILS value corresponding to magnification factor $k = 2, 3, 5$, and 7 are $0.032, 0.047, 0.072$, and 0.087 respectively. Thus we conclude that for a given resist, the ILS can be improved by magnifying the incoming dose and using a thicker CEL film. Dose magnification can be realized in practice using a more powerful light source or longer exposure times. A very high intensity light source endangers the operating life of the (very expensive) lenses, and is a less preferable option. On the other hand, longer exposure times lead to reduction in the overall yield. Hence, we are interested in finding out the maximum mileage (in terms of ILS improvement) possible for a given magnification factor.

It can be proved[16] that for a given value of p, the ILS of the transmitted dose is upper-bounded by p times the ILS of the original incoming dose D_i. In other words,

$$\mathrm{ILS}(D_t(pD_i)) <= p * \mathrm{ILS}(D_i) \tag{9}$$

The above equation is a fundamental relationship which will also be beneficial to evaluate the quality of the CEL material. A good CEL material should be capable of improving the ILS by a full-factor p (particularly for large values of p).

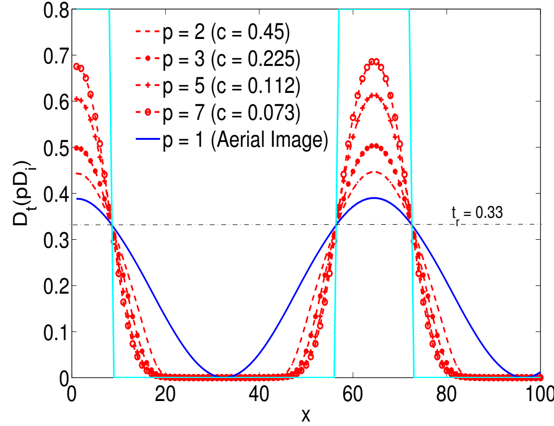

Figure 8. Effect of dose magnification p on the CEL image using fixed resist with threshold ($t_r = 0.33$). Here, $a = 60$ and $t_c = 0.15$.

4.3. Quenchers

The third and final way to improve the ILS is motivated by the fact that the combined CEL image sits on top of a background energy, as observed in Fig. 6. Note that ILS at the desired edge location is evaluated as

$$\text{ILS}(D_t) = \frac{1}{D_t}\frac{dD_t}{dx}.$$

Therefore a possible way to improve the ILS is by adding (base) quenchers to the photoresist. Quenchers are alkaline-based chemicals which can be used to neutralize the extra PAC generated by the (undesired) background energy present in D_t. The above process is equivalent to subtracting a constant q ($q \geq 0$) from D_t thereby effectively shifting the entire modulation curve (indicated in Fig. 6) down. The effect on ILS is as follows:

$$\text{ILS}(D_t - q) = \frac{1}{D_t - q}\frac{d(D_t - q)}{dx} = \frac{1}{D_t - q}\frac{d(D_t)}{dx} > \text{ILS}(D_t)$$

Thus the effective ILS is higher than before.

4.4. Matching with Arsel$^{\text{TM}}$

We now compare the behavior of the proposed CEL model with the measured data curves of Arsel$^{\text{TM}}$(under development by Pixelligent Inc). Fig. 9 indicates the measured optical density (calculated as $\text{OD} = \log(D_i/D_t)$) as a function of input dose D_i. The blue and red curves correspond to the measured OD when D_i is increased from 0 to maximum and decreased back to 0, respectively. The two curves will coincide if the CEL is completely reversible. The graph on the left represents the OD calculated using the proposed model with parameters $a_c = 1.6$, $t_c = 2.5$, and $c = 0.3$. Both graphs indicate a structurally similar behavior; a linear drop in the OD (attributed to bleaching) followed by flattening at higher dose values (attributed to very high $T(D_i)$).

5. CEL AND ILT FOR 2-D PATTERNS

In this section we demonstrate the applicability of CEL for printing 2-D patterns using DEL for $k_1 < 0.25$. The goal is to use ILT framework to synthesize CPL masks for printing the target pattern in Fig. 10 which consists of 40nm features on an 80nm pitch using 193/0.9NA ($k_1 = 0.187$). The target is sampled at 20nm implying that the features are merely two 20nm pixels wide.

Firstly, we want to report that our DEL-ILT algorithm (with the integrated CEL model) did not converge to an acceptable local minima for $k_1 < 0.25$. Therefore, we were unable to perform the automatic pattern

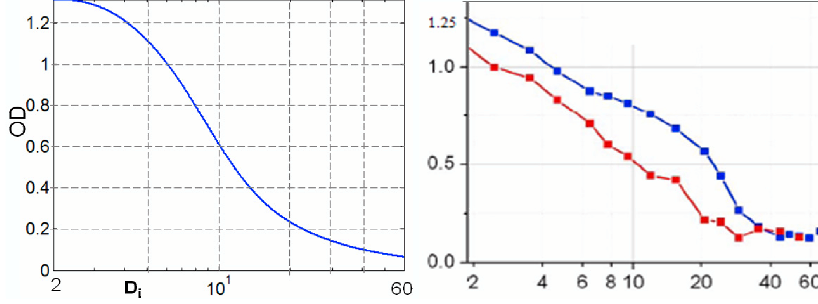

Figure 9. OD versus D_i for the proposed model (left) and the measured data using Arsel $^{\text{TM}}$(right).

decomposition similar to one illustrated in Section 2. We suspect that this may be due to the local gradient-based search technique used for optimization. The algorithm is unable to explore the more complicated search space resulting from $k_1 < 0.25$, and better initialization points may help solve the problem. However, this remains a direction of future work.

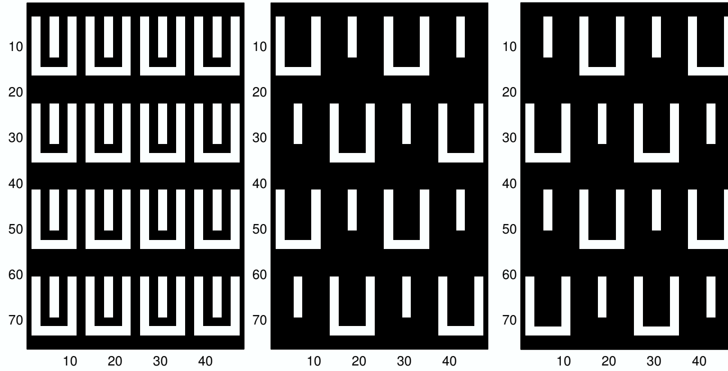

Figure 10. The target pattern consisting of 40nm features on 80 nm pitch and the (manually) decomposed patterns used for individual exposures.

We therefore perform a rule-based pattern decomposition as illustrated in Fig. 10 and employ the single exposure based ILT algorithm to synthesize the CPL masks. The augmented forward model also accounting for the CEL is as follows:

$$\underline{\mathbf{z}} = F(G(p|\mathbf{H}\underline{\mathbf{m}}|^2)), \tag{10}$$

where the function $G(.)$ represents the CEL transmittance function defined in (8). $F(.)$ is a sigmoid function which models the thresholding operation performed by the resist,[20]

$$F(y) = \text{sig}(y) = \frac{1}{1 + \exp(-a_r y + a_r t_r)}.$$

Here a_r and t_r are the slope and threshold parameters of the resist respectively. Thus the forward model in (10) accounts for the magnified incoming aerial image dose, the CEL transferred dose, as well as the resist contour formation. The estimated mask $\hat{\underline{\mathbf{m}}}$ is defined as one which minimizes the L_2 norm of the difference between the target contour $\underline{\mathbf{z}}^*$ and output contour $\underline{\mathbf{z}}$ modeled using (10),

$$\hat{\underline{\mathbf{m}}} = \arg\min_{\underline{\mathbf{m}}} C_1(\underline{\mathbf{m}}) = \arg\min_{\underline{\mathbf{m}}} ||\underline{\mathbf{z}}^* - \underline{\mathbf{z}}||_2^2. \tag{11}$$

The cost function in (11) is still continuous allowing the use of non-linear programming techniques for optimization. We follow our earlier proposed approach,[20] and employ the gradient-descent optimization algorithm to

minimize $C_1(\underline{\mathbf{m}})$. The gradient can be calculated as follows:

$$\nabla C_1(\underline{\mathbf{m}}) = -4a_r p \mathbf{H}^{\mathbf{T}}[(\underline{\mathbf{z}}^* - \underline{\mathbf{z}}) \odot \mathbf{z} \odot (\underline{\mathbf{1}} - \underline{\mathbf{z}}) \odot (\mathbf{H}\mathbf{m}) \odot \underline{\mathbf{q}}], \tag{12}$$

where

$$\underline{\mathbf{q}} = \frac{\underline{1}}{\underline{1} + \exp(-a_c c p |\mathbf{H}\underline{\mathbf{m}}|^2 + a_c t_c)}.$$

Fig. 11 illustrates the results obtained using the CEL-ILT algorithm discussed above. The top row indicates the estimated CPL mask (white = 1 and black = -1), the aerial image, and the CEL image for a single exposure. The simulations parameters were: $a_c = 60$, $t_c = 0.15$, $c = 0.2$, $p = 4$, $a_r = 60$, $t_r = 0.3$. We observe that although the aerial image is very poor, the CEL transmitted image (D_t) has much better contrast, and closely resembles the target. This is because our ILT algorithm is *aware* of the presence of CEL, and estimates the masks taking its action into account. By the end of the first exposure, the CEL transmitted dose is completely absorbed by the photoresist, where it is stored in the form of PAC concentration. The second exposure is performed by simply shifting the mask horizontally by 320nm (see Fig. 10). The bottom row in Fig. 11 indicates that the combined aerial image (the dose received by the resist in the absence of CEL) has no useful modulation. This is expected because $k_{pitch} < 0.5$. However, the linear superposition of the two CEL images shows very good modulation, which will enable patterning of the desired features. The contours at $t_r = 0.3$ indeed indicate good pattern fidelity.

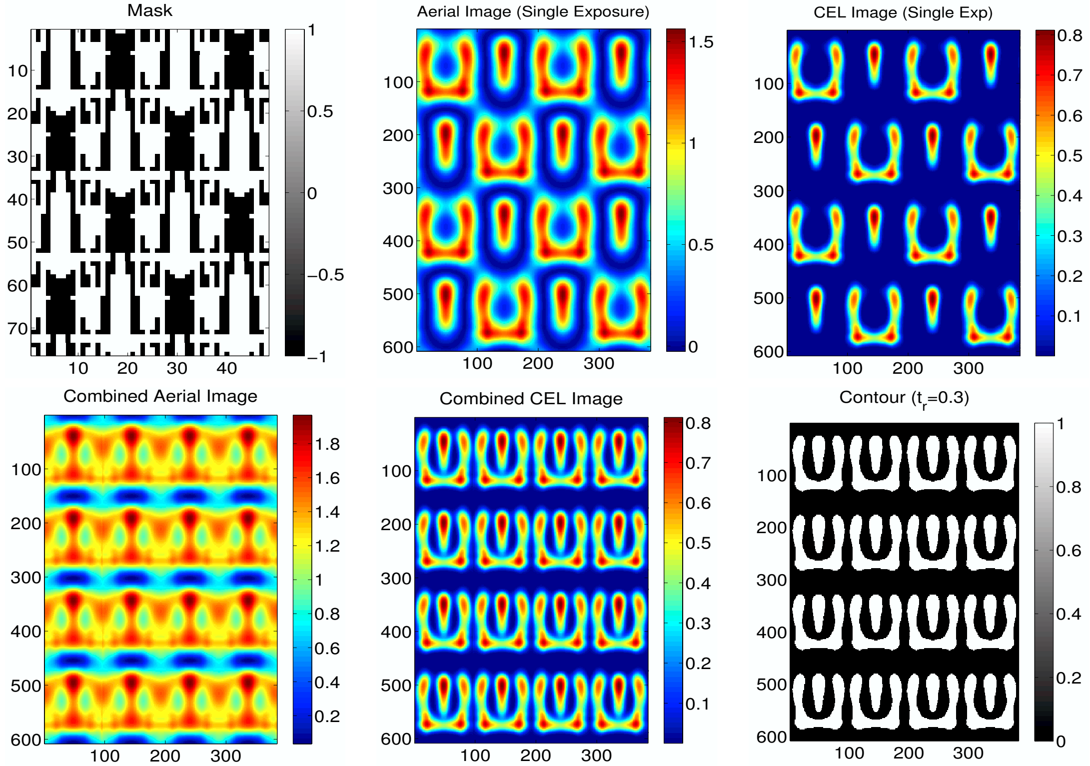

Figure 11. The top row indicates the CEL-ILT results obtained by solving (11). The bottom row indicates the DEL results where the second exposure was performed by shifting the mask by 240nm.

6. TWO-PHOTON ABSORPTION RESIST

The second OSOM material candidate for $k_1 < 0.25$ DEL is two-photon absorption resist. They have been well-known to double the resolution of optical lithography, and were actively explored by Yablonovitch, et al.[24]

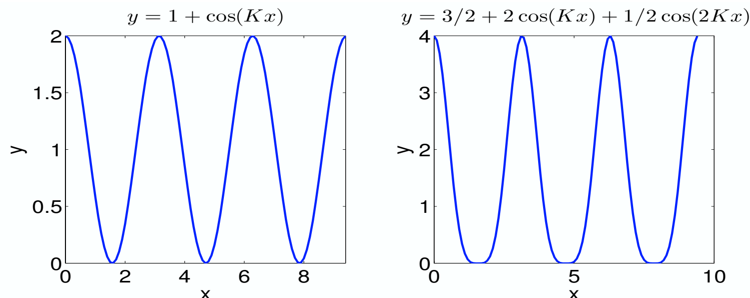

Figure 12. The intensity and square of intensity modulation curves corresponding to the conventional and 2-photon absorption resists respectively.

The left graph in Fig. 12 illustrates the aerial image *intensity* obtained using an interferometric arrangement with 2-coherent beams incident at $\pm\theta$. Therefore, $I(x) = 1 + \cos(Kx)$ where $K = 2k\sin\theta$. For the case of two-photon absorption, the resist responds to the *square* of the intensity. Thus $I^2(x) = 3/2 + 2\cos(Kx) + 1/2 cos2Kx$, which consists of superposition of both the single and double-frequency components. As observed in Fig. 12, the above mixture merely enables patterning at the same resolution as single-photon absorption (although with a better contrast). Therefore, we need to get rid of the linear frequency component in order to enable frequency doubling, and allow $k_{pitch} < 0.5$. Yablonovitch, et al[24] proposed a new (single) exposure arrangement which destroys the stationary interference patterns corresponding to the linear frequency component, leaving behind the double-frequency interference pattern on a background.

A alternative way to enable frequency doubling using 2-photon absorption resists is by employing DEL. In the case of gratings, the second exposure should have an offset of half a period compared to the first. Therefore the combined contribution from the two exposures is given as follows:

$$\begin{aligned} I_1^2(x) + I_2^2(x) &= [1 + \cos(Kx)]^2 + [1 + \cos(Kx + \pi)]^2 \\ &= [1 + 2\cos(Kx) + \cos^2(Kx)] + [1 - \cos(Kx)]^2 \\ &= [1 + 2\cos(Kx) + \cos^2(Kx)] + [1 - 2\cos(Kx) + \cos^2(Kx)] \\ &= 2 + 2\cos^2(Kx) \\ &= 3 + \cos(2Kx) \end{aligned}$$

We observe that by merely shifting and adding $I^2(x)$, the linear frequency component cancels out, leaving behind only the double-frequency component with a DC background. Thus 2-photon absorption resists are naturally suitable to DEL. Yet, we are not aware of materials with suitably large 2-photon absorption cross-section value at wavelength of interest. As a result one would need very high power at the wafer plane to obtain significant two-photon excitation rates with existing materials, making it practically possible, but economically unsuitable for high volume manufacturing.

7. CONCLUSION AND FUTURE WORK

In this paper we discussed two different paradigms of double exposure single development lithography. For $k_1 > 0.25$, we discussed a new approach of using ILT to decompose the aerial image and simultaneously estimating the two masks best suited for the purpose. The combined aerial image has very good contrast and will enable patterning close to $k_1 = 0.25$. For the case of $k_1 < 0.25$, we identified CEL and two-photon absorption resists as two potential candidates. We presented the mathematical model of a desirable reversible CEL material (neglecting the reflections from the substrate) and discussed several ways of improving the aerial image slope. A comparison with Arsel™(by Pixelligent Inc.) provided encouraging results. Reversibility of the CEL film was identified as the key enabler for the success of DEL. We also presented simulation results for patterning 1-D and 2-D features using a combination of CEL, DEL, and ILT. For two-photon absorption resist, the biggest challenge is the unavailability of a material with necessarily high cross-section for 2-photon absorption.

The proposed CEL model assumes 100% opacity and 100% transparency for unbleached and fully bleached states respectively, which is impractical. The future work consists of refining the CEL model to incorporate the practical transmittance values of the CEL film. We also hope to carry out physical experiments using CEL and report the results in our future publications.

REFERENCES

1. A. Biswas, J. Li, J. Hiserote, and L. Melvin III, *Extension of 193nm dry lithography to 45-nm half-pitch node: Double exposure and double processing technique*, BACUS Symposium on Photomask Technology, Proc. SPIE, vol. 6349, 2006.
2. T. Chiou, A. Chen, S. Hsu, M. Eurlings, and E. Hendrick, *Development of automatic OPC treatment and layout decomposition for double dipole lithography for low-k1 imaging*, Advanced Microlithography Technologies, Proc. SPIE, vol. 5645, 2005, pp. 21–31.
3. A. Erdmann, R. Farkas, T. Fuhner, B. Tollkuhn, and G. Kokai, *Towards automatic mask and source optimization for optical lithography*, Optical Microlithography, Proc. SPIE, vol. 5377, 2004, pp. 646–657.
4. J. Park et al, *Application challenges with double patterning technology beyond 45nm*, BACUS Symposium on Photomask Technology, Proc. SPIE, vol. 6349, 2006.
5. M. Fritze, B. Tyrrell, D. Astolfi, R. Lambert, D. Yost, A. Forte, S. Cann, and B. Wheeler, *Subwavelength optical lithography with phase-shift-mask*, Lincoln Laboratory Journal **14** (2003), 237–250.
6. L.F. Halle, *A water soluble contrast enhancement layer*, Journal of Vaccuum Science and Technology B **3** (1985), 323–326.
7. M. Hasegawa, A. Suzuki, K. Saitoh, and M. Yoshii, *New approach for realizing $k_1 = 0.3$ optical lithography*, Symposium on Photomask and X-Ray Mask Technology, Proc. SPIE, vol. 3748, 1999, pp. 278–287.
8. S. Hsu, J. Park, D. Broeke, and J. Chen, *Double exposure technique for 45nm and beyond*, BACUS Symposium on Photomask Technology, Proc. SPIE, vol. 5992, 2005.
9. Y. Liu and A. Zakhor, *Optimal binary image design for optical lithography*, Optical Microlithography, Proc. SPIE, vol. 1264, 1990, pp. 401–412.
10. W. Loong and H. Pan, *A direct approach to the modeling of polydihexisilane as a contrast enhancement material*, Journal of Vaccuum Science and Technology B **8** (1990).
11. C. Mack, *Contrast enhancement techniques for submicron optical lithography*, Journal of Vaccuum Science and Technology A **5** (1987).
12. C. Noelscher, M. Heller, B. Habets, M. Markert, U. Scheler, and P. Moll, *Double line shrink lithography at* $k_1 = 0.16$, Microelectronic Engineering **83** (2006), 730–733.
13. Y. Oh, J. C. Lee, and S. Lim, *Resolution enhancement through optical proximity correction and stepper parameter optimization for 0.12-μ mask pattern*, Optical Microlithography, Proc. SPIE, vol. 3679, 1999, pp. 607–613.
14. W. Oldham, *The use of contrast enhancement layers to improve the effective contrast of positive photoresist*, IEEE Transactions on Electron Devices **34** (1987), 247–251.
15. E. Ong, B. Singh, R. Ferguson, and A. Neureuther, *Comparison of proximity effects in contrast enhancement layer and bilayer resist processes*, Journal of Vaccuum Science and Technology B **5** (1987), 443–448.
16. A. Poonawala, *Single and double exposure inverse lithography mask design for optical lithography (in preparation)*, Ph.D. thesis, University of California, Santa Cruz, 2007.
17. A. Poonawala and P. Milanfar, *Double exposure mask synthesis using inverse lithography*, Submitted to Journal of Microlithography, Microfabrication and Microsystems (Preprint available online).
18. ———, *Prewarping techniques in imaging: Applications in nanotechnology and biotechnology*, Electronic Imaging, Proc. SPIE, vol. 5674, 2005, pp. 114–127.
19. ———, *OPC and PSM design using inverse lithography: A non-linear optimization approach*, Optical Microlithography, Proc. SPIE, vol. 6154, 2006, pp. 114–127.
20. ———, *Fast and low-complexity mask design in optical microlithography - an inverse imaging problem*, To appear for Publication in IEEE Transactions on Image Processing (2007).
21. S. Sayegh and B. Saleh, *Image design: Generation of a prescribed image at the output of a bandlimited system*, IEEE Transcation on Pattern Analysis and Machine Intelligence **5** (1983), 441–445.

22. S. Sayegh, B. Saleh, and K. Nashold, *Image design: Generation of a prescribed image through a diffraction limited system with high-contrast recording*, IEEE Transaction on Acoustics, Speech and Signal Processing **33** (1985), 460–465.
23. S. Sherif, B. Saleh, and R. Leone, *Binary image synthesis using mixed linear integer programming*, IEEE Transactions on Image Processing **4** (1995), 1252–1257.
24. E. Yablonovitch and R. Vrijen, *Optical projection lithography at half the rayleigh resolution limit by two-photon exposure*, Optical Engineering **38** (1999), 334–338.